JOURNAL OF AIRCRAFT
Vol. 35, No. 5, September–October 1998

Fin Buffet Pressure Evaluation Based on Measured Flowfield Velocities

Christian Breitsamter* and Boris Laschka†
Technische Universität München, 85747 Garching, Germany

A method to predict fin buffet aerodynamic loads is developed based on measured fluctuating velocity fields only. This has been investigated for a model of a high-performance, single-finned, delta-canard configuration. The time-dependent velocity field is measured in the fin region, resulting in a detailed description of the properties of the buffet-inducing quantities. A modified lifting surface method is used to evaluate the unsteady fin surface pressures. It is based on the amplitude spectra of local fin incidence calculated from the measured velocities. Consequently, rms and spectral densities of fluctuating surface pressure and normal force are obtained. It is shown that the fin buffet pressures increase significantly with increasing incidence. At high incidences the buffet load spectra exhibit strong narrow-band peaks. They correspond to the quasiperiodic fluctuations present in the breakdown flow of wing and canard leading-edge vortices approaching the midsection. The results that were obtained agree very well with direct-measured fin buffet pressure. This gives strong evidence that fin buffet loads can be determined with adequate accuracy by the approach suggested in this paper.

Nomenclature

A, B = Fourier coefficients
A_F, A_{P_i} = surface area of fin, area of ith panel on fin
c_N = normal force coefficient
c_p = pressure coefficient
c_r = wing root chord, m
f = frequency, Hz
f_M = sampling frequency, Hz
f_T = low-pass filter frequency, Hz
K = Kernel function of lifting surface integral equation
k = reduced frequency, fl_μ/U_∞
k' = reduced frequency, $(fc_r/U_\infty)\sin\alpha$
l_μ = wing mean aerodynamic chord, m
Ma = freestream Mach number
N = number of sampled values
N_p = number of panels
n_f = number of frequency intervals
p = (surface) pressure, N/m^2
q_∞ = freestream dynamic pressure, N/m^2
Re = Reynolds number, $U_\infty l_\mu/\nu$
S = power spectral density, 1/Hz
S_v = power spectral density of v', (m/s)^2/Hz
s = wing semispan, m
s_F = fin span, m
T = sampling time, s
U_∞ = freestream velocity, m/s
u, v, w = streamwise, lateral, and vertical velocity components, respectively, m/s
X, Y = dimensionless (fin) coordinates, referred to local chord and span, respectively
x, y, z = streamwise, lateral, and vertical coordinates, respectively, m
α = aircraft angle of attack, deg
α_F = fin local incidence, deg
β = aircraft angle of sideslip, deg
Δc_p = differential pressure coefficient
Λ, λ = aspect ratio, taper ratio
ν = kinematic viscosity, m^2/s; dihedral, deg
ς = leading-edge sweep, deg
ω = angular frequency, Hz

Subscripts
C = canard
F = fin
rms = root-mean-square value
v, h = leading edge, trailing edge, respectively
W = wing

Superscripts
$\bar{}$ = time-averaged quantities
$'$ = fluctuation quantities; lifting surface coordinates
$\hat{}$ = amplitude

Presented as ICAS Paper 96-1.6.2 at the 20th Congress of the International Council of the Aeronautical Sciences, Sorrento, Napoli, Italy, Sept. 9–13, 1996; received May 18, 1997; revision received March 15, 1998; accepted for publication May 21, 1998.

*Dr.-Ing., Akademischer Rat, Lehrstuhl für Fluidmechanik.
†Full Professor of Fluid Mechanics, Lehrstuhl für Fluidmechanik. Fellow AIAA.

Introduction

FOR the generation of modern fighter aircraft fitted with slender wing geometry and canards as well as conventional aft control surfaces, the capability of supermaneuvering has been well demonstrated. Supermaneuvering is associated with controlled flight at incidences near or exceeding maximum lift. In that flight regime the aircraft may experience severe fin buffet because of the highly turbulent flow caused by burst leading-edge vortices.[1–8] The induced narrow-band aerodynamic loads frequently excite the fin structure at the natural frequencies, thus constituting a threat to the fin structural integrity. Corrective actions may be required to ensure both vibration-free control and long fatigue life.[9] In this context the physics of the interaction of a streamwise vortex with a thin plate as a source of turbulent buffeting were studied in detail by Mayori and Rockwell,[10] Cambazoglu et al.,[11,12] and Wolfe et al.[13]

In particular, with twin-tailed fighter aircraft (F-15, F/A-18) the fin buffet problem became a crucial issue,[14,15] and the single-finned X-29 and X-31 research aircraft were also affected.[16] Comprehensive investigations have been conducted aimed at understanding and reducing the buffet loads.[17–20] The majority of data is related to small-scale wind-tunnel tests

complemented by results of some full-scale model tests[21] and corroborated by flight test data.[22]

An extensive investigation on the fin flow environment of a delta-wing model with canard stabilizer and a single centerline fin was started at the Lehrstuhl für Fluidmechanik of the Technische Universität München. The turbulent flow structure in the fin region was well defined by the spatial and temporal characteristics of the time-dependent flow velocities, resulting in a general treatment of the fin buffet problem. In Ref. 4 results at symmetric freestream are discussed, flow properties at sideslip are reported in Ref. 5. The behavior of the flow quantities is shown to be significant for the vortex breakdown flowfield. An annular structure assigned to the remaining swirling vortex sheet is the locus of maximum turbulence intensity. There, the fluctuations are channeled into a narrow band arising from a helical mode instability.[23] The detailed flowfield surveys are of particular use for the development and validation of computational prediction methods.[24,25]

All response analyses to date have relied on experimental data for the pressure inputs.[7,8,26] The stress analyses and fatigue assessments used data for fin aerodynamic loads obtained by direct steady and unsteady pressure measurements at sufficient points on the fin surface. Experiments were conducted on rigid and flexible wind-tunnel models employing the results for the full-scale aircraft design.[7,8]

In general, Reynolds number and Mach number matching is required to extrapolate small-scale data to flight conditions. For fixed leading-edge flow separation and high turbulence intensity within the breakdown flowfield, the influence of Reynolds number, however, is rather small. At the incidences of interest, maneuvering aircraft would experience large normal loads, as most flight is limited to lower Mach numbers.[9] For this case it is shown that buffet spectra could be extrapolated to large ranges of velocities and model sizes, and that they could be used to predict flight loads.[7,8]

The present investigation focuses on the prediction of fin buffet aerodynamic loads. The buffet excitation input is defined by the lateral turbulence intensity and related power spectral density distributions. A modified lifting surface method based on Ref. 27 is used to evaluate unsteady fin surface pressure. Hence, the prediction method is based only on features of the flowfield that are dependent on the aircraft configuration and aerodynamic conditions such as Mach number, angle of attack, and angle of sideslip. The possibility to carry out flowfield measurements at any aircraft model leads to great flexibility, particularly, in an early design stage. In this phase extensively instrumented and costly fin models that cannot be easily adapted to design modifications may be downgraded.

Measurement Technique and Test Program

Model and Facility

The wind-tunnel model that was used represents a high-agility aircraft of canard-delta wing type (Fig. 1). Major parts of the steel model were a nose section, a front fuselage including rotatable canards and a single place canopy, a center fuselage with a delta-wing section and a through-flow double air intake underneath, and a rear fuselage including the nozzle section. The single fin was part of an insert that was bolted to the rear fuselage. For the flowfield surveys, the leading- and trailing-edge flap deflections and the canard setting angle were set at 0 deg. The model was sting mounted on its lower surface from a moving support strut. This arrangement enables flowfield measurements to be free from interference. The computer-controlled model support provides an incidence range from 0 to 31.5 deg, and models may be yawed and rolled 360 deg.

The experiments were conducted in a Göttingen-type low-speed wind tunnel with an open circular test section of 1.5 m diameter. Maximum usable velocity was 55 m/s. Turbulence intensity ranged from 0.3–0.4%.

$2s = 0.740$ m	$\varphi_W = 50°$
$l_\mu = 0.360$ m	$\varphi_C = 45°$
$\Lambda_W = 2.45$	$\lambda_W = 0.14$

$s_F = 0.47\ s$	$\varphi_F = 54°$
$\Lambda_F = 1.38$	$\lambda_F = 0.19$

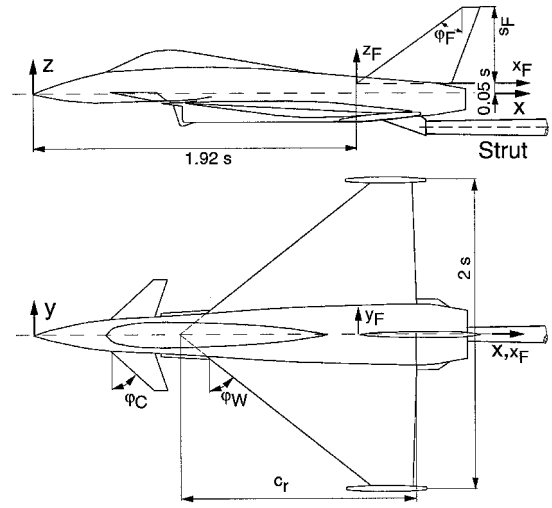

Fig. 1 Geometry of delta-canard model.

Measurement of Time-Dependent Velocity

Dual-sensor hot-wire probes (Dantec 55P61) were used to measure the fluctuating velocity components. The probes were operated by a multichannel, constant-temperature anemometer system (Dantec C). By means of its signal conditioner modules, bridge output voltages were low-pass filtered at 1000 Hz before digitization and amplified for optimal signal levels. The signals were then digitized with 12-bit precision through a 16-channel simultaneous-sampling A/D converter. The sampling rate for each channel was set to 3000 Hz, giving a Nyquist frequency of 1500 Hz. The sampling time was 38.4 s. Thus each sample block contained 115,200 points in the time domain, producing 57,600 points in the complex frequency domain. The sampling parameters were achieved by preliminary tests to ensure that all significant flowfield phenomena were detected. Statistical accuracy of the calculated quantities was considered as well. The sampling parameters are related to a statistical error of 0.2, 1, and 2.5% for the mean and standard deviation and spectral density estimation, respectively.

To determine all three velocity components (u, v, and w), two triggered traverse sweeps are necessary to adjust the cross-wire plane: once horizontal and once vertical against the main flow direction. Each digitized and temperature-corrected voltage-pair of the corresponding probe positions was converted to evaluate the time-dependent velocity vector. The method used is based on lookup tables derived from the full velocity- and flow-angle-dependent calibration of the sensors. A detailed description is given in Refs. 28 and 29.

Conduction of Tests

Flowfield measurements were performed at discrete points in the fin region corresponding to the lifting surface collocation points (Fig. 2). The fin section was removed to encounter only the flowfield input. Previous investigations for the fin-off and fin-on cases have shown that at zero sideslip only negligible effects on the vortex structures could be observed.[4,30] Consequently, for the angles of attack investigated, there are only very small differences between fin-off and fin-on regarding turbulence intensities as well as spectral quantities at stations close to the midsection.[30] At small sideslip (β = 5 deg) the flowfields for fin-off and fin-on are not completely the same. However, turbulence intensities and even spectral quantities do not differ significantly.[31]

The tests were made at five angles of attack, namely, α = 20, 25, 28, 30, and 31.5 deg, and at sideslip β = 0 and 5 deg. The freestream reference velocity U_∞ was held constant at 40 m/s, corresponding to Ma = 0.12. This gives a Reynolds number of $Re = 0.97 \times 10^6$, based on the wing mean aerodynamic chord for all of the results presented. Further test section conditions were ambient static pressure and temperature. At all tests, the turbulent boundary layers were present at wing and control surfaces proved by shear-stress sensitive liquid crystal measurements.[29]

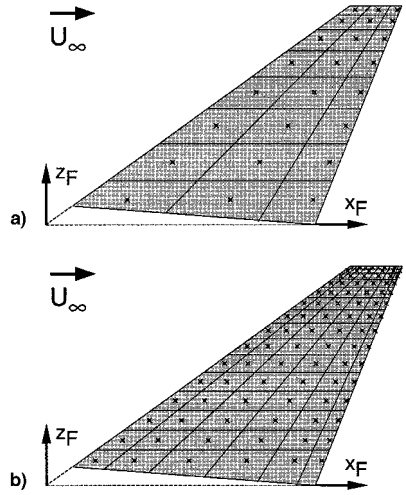

Fig. 2 Measurement stations in the fin region and fin collocation points, respectively: a) 3 × 8 points and b) 6 × 15 points.

Buffet-Inducing Flowfield

To quantify the buffet excitation level the flowfield is carefully described by the velocity fluctuations. For a single fin the lateral velocity mainly causes buffeting, whereas for a twin-fin with dihedral, both the lateral and the vertical velocity contribute.

Lateral Turbulence Intensity Distributions

The rms values of fluctuating velocity v_{rms} provide a measure of the intensity of the fluctuating input. They are typically nondimensionalized by U_∞ to present the relative turbulence intensity in terms of percent of freestream. For the fin survey, Figs. 3 and 4 contain contours of lateral rms velocity for various α and β. Based on results of Refs. 4 and 5, simplified schematics of the cross-sectional turbulence intensities are also shown. These sketches depict the evolution of the incident, burst vortex systems that determine mainly the rms pattern of the fin region.

At symmetric freestream the rms velocity fluctuations at α = 20 deg are relatively low (Fig. 3a). They are characterized by a homogeneous distribution over the whole fin section. At this incidence the fin flow environment is only slightly affected by the port and starboard wing leading-edge vortices (WLVs) or canard vortex systems. The latter consists of a leading-edge vortex (CLV) and a trailing-edge vortex (CTV). The canard vortex system keeps its structure downstream, still behind the wing trailing edge.[29] With increasing incidence the burst WLVs

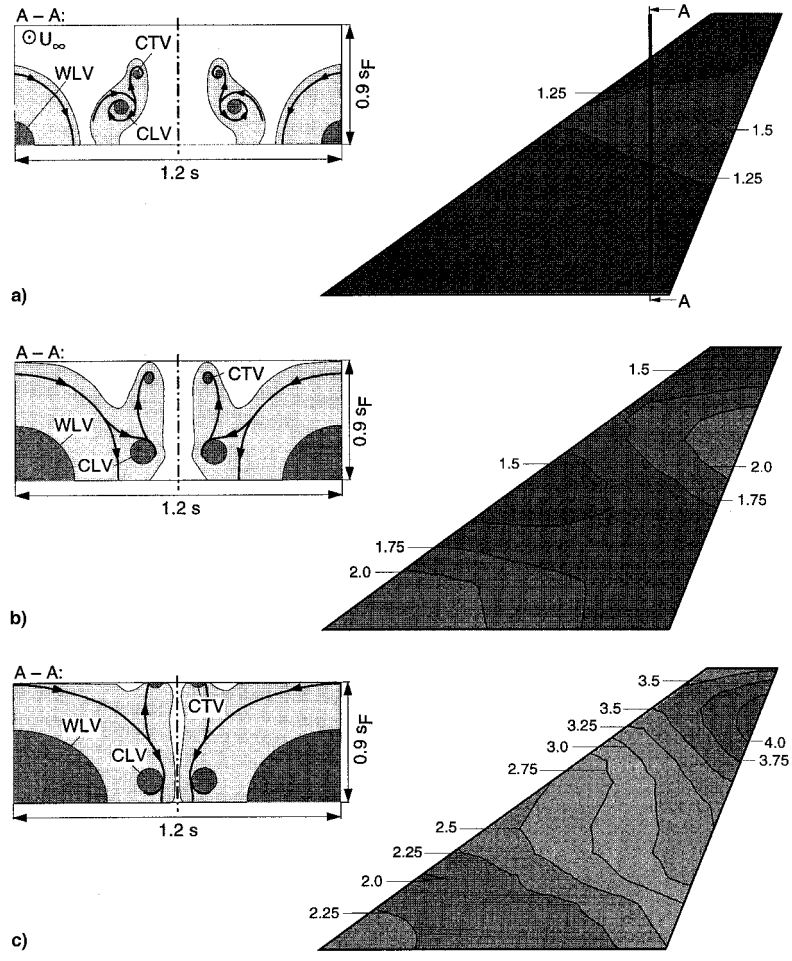

Fig. 3 v_{rms}/U_∞ at α = a) 20, b) 25, and c) 30 deg and β = 0 deg (values in percent). A-A: sketch of vortex flow features in a plane normal to the fin surface at 95% fin root chord based on rms patterns of Ref. 4, view from behind, light gray areas: shear-layer regions ($v_{rms}/U_\infty \approx$ 3–12%), dark gray areas: core regions ($v_{rms}/U_\infty \approx$ 8–14%).

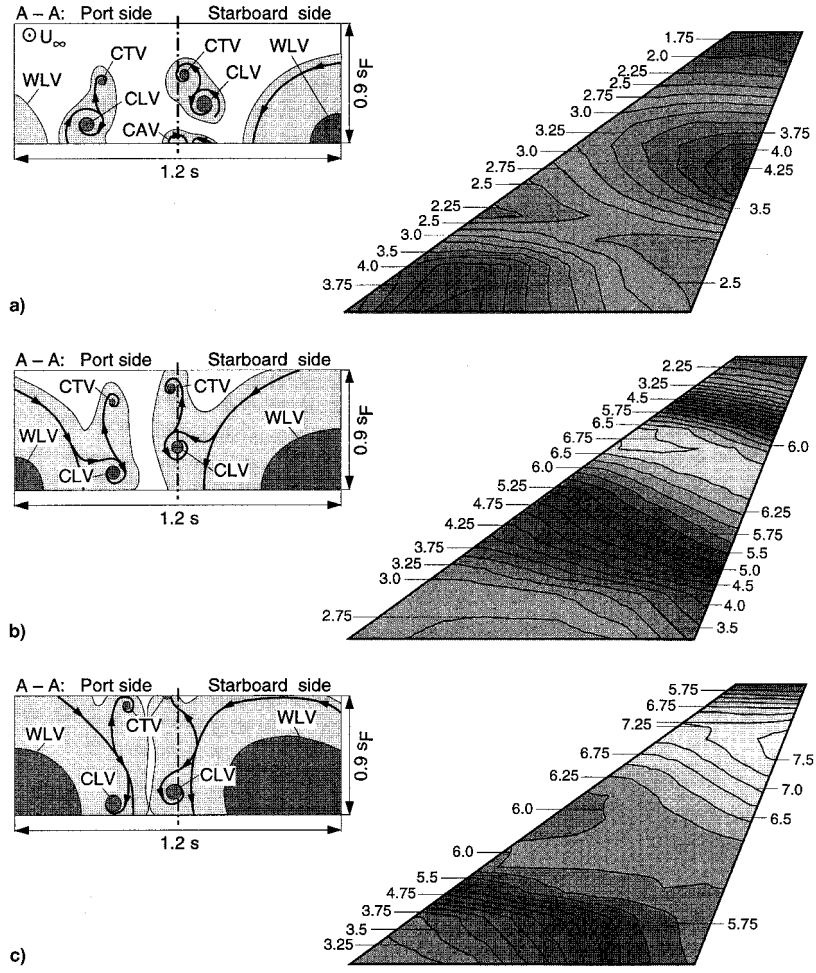

Fig. 4 v_{rms}/U_∞ **at** α **= a) 20, b) 25, and c) 30 deg and** β **= 5 deg (values in percent). A-A: sketch of vortex flow features in a plane normal to the fin surface at 95% fin root chord based on rms patterns of Ref. 5, view from behind, light gray areas: shear-layer regions (**$v_{rms}/U_\infty \approx$ **3–12%), dark gray areas: core regions (**$v_{rms}/U_\infty \approx$ **8–14%).**

expand and move inboard and upward. By wing influence the canard vortex systems are shifted inward and downward. Consequently, the CLVs merge completely with the inboard part of the WLV sheets, whereas the CTVs are detached upward.[4] The fin flowfield takes on a dramatically different character at α = 25 deg, shown by considerably increased rms values (Fig. 3b). Maximum values in v_{rms}/U_∞ are found at the fin root close to its leading edge, and at 65% span close to its trailing edge. The first values stem from the CLVs, and the second ones from the CTVs. At α = 30 deg, the process of vortex interaction described earlier continues. It results in maximum rms values near the tip of the fin (Fig. 3c).

At sideslip, β = 5 deg, the starboard wing and canard vortices are shifted inboard, dominating the flow behavior in the midsection.[5] At α = 20 deg, the rms values have increased to three times the level of symmetric flow conditions (Fig. 4a). A vortex pair [canopy vortex pair (CAV)] shed at the canopy evoke an rms maximum at the root of the fin. A second rms maximum located near the midspan close to the trailing edge is caused by the starboard canard vortex system. The pattern in lateral turbulence intensity becomes very different at α = 25 deg (Fig. 4b). There, the rms values are the largest in a region at 60% span, covering a small area from the leading to the trailing edge. Values of v_{rms}/U_∞ decrease toward the root and tip of the fin. The region of maximum rms values is related to the starboard WLV sheet approaching the midsection, in particular, to that part where the starboard CLV is embedded. At α = 30 deg, the region of maximum lateral turbulence intensity has grown in size and strength (Fig. 4c). It is placed closer to the fin tip because of the starboard WLV, which moves upward and becomes enlarged.

Character of the Spectral Content

Velocity spectra are shown in Fig. 5 for α = 25 and 30 deg and β = 0 and 5 deg at station A 17. The power spectral density is evaluated with 512 band-averaged and hanning-windowed frequency intervals. For the Nyquist frequency of 1500 Hz the frequency resolution is 2.93 Hz.

After the rapid expansion of the burst vortex core the flow changes to a highly turbulent swirling state, where large narrow-band velocity fluctuations occur.[4,5] In the midsection, a narrow-band concentration of kinetic turbulent energy is detected the first time at α = 25 deg (Figs. 5a and 5c). As substantiated in Ref. 4, the distinct frequency peak centered around k = 0.9 coincides with the sharp peaks detected in the shear-layer velocity spectra of the burst WLVs. In Ref. 23 it is pointed out that after vortex breakdown the flow is subject to a helical mode instability producing quasiperiodic velocity fluctuations. That in turn gives rise to coherent pressure fluctuations. At α = 30 deg, the fin flow more extensively encounters the vortex breakdown flow, resulting in pronounced frequency peaks of k = 0.6–0.8 (Fig. 5b). The spectra depict a second frequency hump around k = 3.0, which refers to the canard vortex system. During the merging process of wing and canard vortex sheets, both vortex burst frequencies are present. At sideslip the fin flow comes in strong contact with the vortex core flow, the spectra becomes widened, and the overall level of turbulent kinetic energy increases (Fig. 5d).

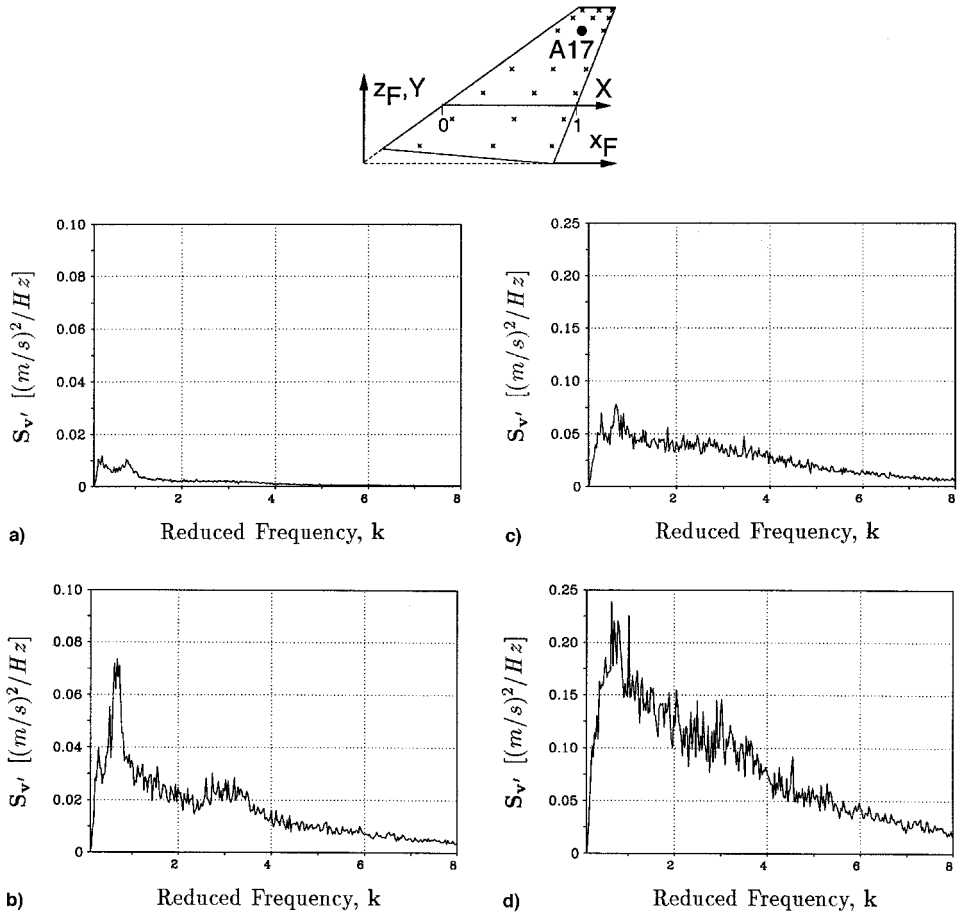

Fig. 5 Spectra of fluctuating lateral velocity $S_{v'}$ at station A 17 ($X = 0.611$, $Y = 0.831$) for various α and β: a) $\alpha = 25$, $\beta = 0$ deg, $v_{rms}/U_\infty = 1.41\%$; b) $\alpha = 30$, $\beta = 0$ deg, $v_{rms}/U_\infty = 3.41\%$; c) $\alpha = 25$, $\beta = 5$ deg, $v_{rms}/U_\infty = 4.19\%$; and d) $\alpha = 30$, $\beta = 5$ deg, $v_{rms}/U_\infty = 7.37\%$.

Evaluation of Buffet Pressure

As shown in the previous section, the statistical properties of the buffet-inducing turbulent flowfield are well known. Therefore, classical unsteady aerodynamic theory might be suitable for predicting the pressures and airloads produced thereby. In the present study a modified unsteady lifting surface method is applied. Fundamentals are given by Laschka.[27]

Integral Equation

The Küssner integral equation reflects the relation between the angle-of-attack and pressure distributions of harmonically oscillating lifting surfaces

$$\alpha(x, y) = \frac{1}{8\pi} \int_{-s}^{s} \int_{x_v(y')}^{x_h(y')} \Delta c_p(x', y') K(x, y, x', y')\, dx'\, dy' \qquad (1)$$

Eq. (1) can as well be used for a static surface (fin) in a flowfield, where the normal-wash as a function of x and y changes harmonically. The unknown quantity is the pressure distribution Δc_p. It denotes the pressure difference between both sides of surface Δp, referred to freestream dynamic pressure q_∞

$$\Delta p(x, y)/q_\infty = \Delta c_p(x, y) e^{i\omega t} \qquad (2)$$

Because of harmonic motions, the amplitude of the angle-of-attack distribution $\hat{\alpha}(x, y)$ yields

$$\alpha(x, y, t) = \hat{\alpha}(x, y) e^{i\omega t} \qquad (3)$$

According to Refs. 27 and 32, the Kernel function $K(x, y, x', y')$ was reduced to a form suitable for numerical and analytical solutions. The unknown pressure distribution $\Delta c_p(x, y)$ is approximated by means of adequate functions in chordwise and spanwise directions. After introducing those functions into the integral equation [Eq. (1)], a system of linear equations results. The normal-wash condition may be fullfilled in a number of collocation points (X, Y), which correspond to the number of functions. Modifications were made to consider high-frequency input and an arbitrary number of collocation points in chord direction. The course of solution is described in detail in Ref. 29.

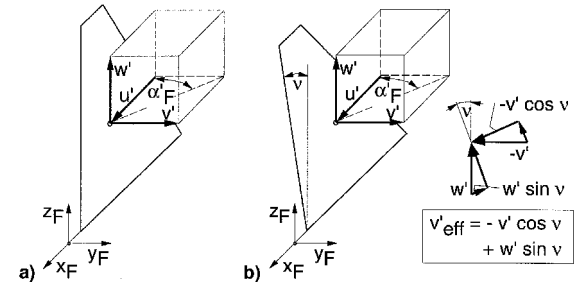

Fig. 6 Local fluctuating fin incidence α'_F: a) Centerline fin: $\alpha'_F = \tan(v'/u')$ and b) fin with dihedral ν: $\alpha'_F = \tan(v'_{eff}/u')$.

Buffet Excitation Input

The local time-dependent incidences $\alpha'_F(X, Y)$ responsible for fin buffet can be easily calculated from the measured fluctuating velocities present in a plane perpendicular to the fin surface. This is shown in Fig. 6 with respect to a single centerline fin as well as to a twin-fin with dihedral.

Because of the concept of small disturbances in linear potential theory, one can infer that the magnitude of the fluctuating incidences is in the vicinity of 7 deg or less. This is

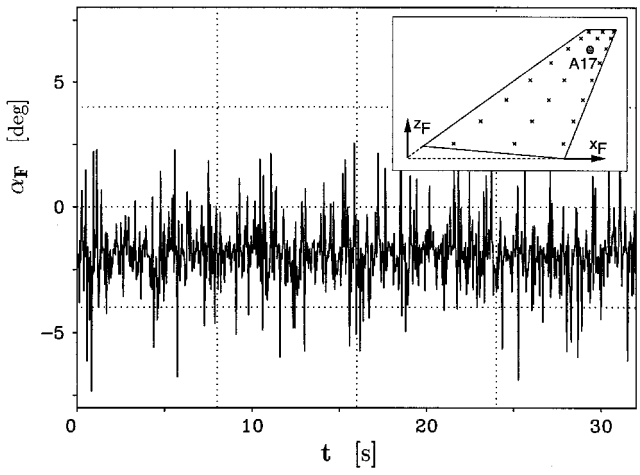

Fig. 7 Time series of fin local incidence α_F measured at station A 17 ($X = 0.611$, $Y = 0.831$) at $\alpha = 31.5$ and $\beta = 0$ deg.

substantiated by a representative plot of the α_F time series (Fig. 7). The mean incidence $\bar{\alpha}_F$ of the fin(s) at zero sideslip is known to be quite small. Regarded as a source of interference airloads, the turbulence seems therefore unlikely to cause flow separation. For the tested centerline fin this is proved by liquid crystal measurements.[29] However, the highly turbulent breakdown flowfield transfers its unsteadiness by induction effects to the attached flow on the fin. At sideslip or at twin-fin stations, the turbulence intensity increases strongly. Regions of highly unsteady and even totally separated flow was, e.g., found at the surfaces of F/A-18 twin-fins at high α.[33] The proposed method will not give satisfactory results if distinct regions of separated flow occur on the fin surfaces.

Adopting the lifting surface method the local incidences $\alpha'_F(t)$ may be expressed as a series of superimposed harmonically oscillations derived from Fourier analysis of discrete values.[34] The sample record $\alpha'_F(t)$ (zero mean) is of finite length T, the fundamental period of the data. The record is sampled at an even number of N equally spaced points a distance $1/f_M$ apart; $T = N/f_M$

$$\alpha'_{F_n} = \alpha'_F\left(n\,\frac{1}{f_M}\right), \qquad n = 1, 2, \ldots, N \tag{4}$$

For a finite version of a Fourier series that will pass through these, N data values hold

$$\alpha'_{F_n} = \sum_{q=1}^{N/2} A_q \cos\left(\frac{2\pi qn}{N}\right) + \sum_{q=1}^{(N/2)-1} B_q \sin\left(\frac{2\pi qn}{N}\right)$$

$$A_q = \frac{2}{N}\sum_{n=1}^{N} \alpha'_{F_n} \cos\left(\frac{2\pi qn}{N}\right), \qquad q = 1, 2, \ldots, \frac{N}{2} - 1 \tag{5}$$

$$B_q = \frac{2}{N}\sum_{n=1}^{N} \alpha'_{F_n} \sin\left(\frac{2\pi qn}{N}\right), \qquad q = 1, 2, \ldots, \frac{N}{2} - 1$$

A finite range Fourier transform can be used to compute the coefficients A_q and B_q. The Fourier components A_j of the selected frequencies f_j are defined by

$$f_j = j/T, \qquad j = 0, 1, \ldots, N-1 \tag{6}$$

$$A_j = \frac{A(f_j, T)}{1/f_M} = \sum_{n=0}^{N-1} \alpha'_{F_n} e^{-i(2\pi jn/N)} \tag{7}$$

where $1/f_M$ has been included with $A(f_j)$ to have a scale factor of unity before summation. Note that results are unique only out to $j = N/2$ because the Nyquist cutoff frequency occurs at this point. The power spectral density $S_{\alpha'_F}(X, Y)$ and the cross-spectral density $S_{\alpha'_F}(X_R, Y_R; X, Y)$ becomes

$$S_{\alpha'_F}(X, Y, f_j) = (2/Nf_M)\left|A_j(X, Y)\right|^2 \tag{8}$$

$$S_{\alpha'_F}(X_R, Y_R, X, Y, f_j) = (2/Nf_M)A_j^*(X_R, Y_R)A_j(X, Y) \tag{9}$$

where $A^*(f_j)$ is the complex conjugate of $A(f_j)$. For scaling nondimensionalized spectra can be obtained referring to the rms value, the freestream velocity and the wing mean aerodynamic, i.e. $[(S_{\alpha'_F}/\overline{\alpha'^2_F})\cdot(U_\infty/l_\mu)]$. The reduced frequency k is used as well.

To reduce the amount of considered discrete frequencies the relevant frequency range of the incidence spectra $0 \le f \le f_T$ is divided into $n_f = 512$ intervals Δf. For each centered discrete frequency

$$f_l = \frac{(2l+1)f_T}{2n_f}, \qquad l = 0, 1, \ldots, n_f - 1 \tag{10}$$

the amplitude $\hat{\alpha}'_F(f_l)$ is determined from the power spectral density $S_{\alpha'_F}(f_l)$

$$\hat{\alpha}'_F(f_l) = \sqrt{2\int_{f_l-\Delta f/2}^{f_l+\Delta f/2} S_{\alpha'_F}(f)\,\mathrm{d}f} \tag{11}$$

carried out at all collocation points (X, Y). This implies the conservative assumption of 100% spatial correlation.

To refine the approach, cross spectra are taken into account [Eq. (9)]. The cross spectra are based on further measurements carried out with two hot-wire probes, with one probe held fixed at the reference point (X_R, Y_R). For each discrete frequency f_l the related phase spectra provide a possible phase shift in fin local incidence between the measurement stations regarded. Hence, the real part of fin local incidence taken from the amplitude spectra is complemented by an imaginary part obtained from the phase spectra.

Results and Discussion

Calculated rms Differential Pressure

The rms values of the fluctuations in fin differential pressure $\Delta c_{p_{\mathrm{rms}}}$ are shown in Figs. 8 and 9, referring to the conditions of Figs. 3 and 4. The pattern of intensity of the unsteady pressure fluctuations corresponds to that of fluctuating lateral velocity. This is caused by the linear relationship between the amplitude functions of local incidence and pressure [Eq. (1)]. At $\alpha = 20$ and $\beta = 0$ deg, the pressure fluctuations are very low as the burst leading-edge vortices are less expanded and located outward (Fig. 8a). At $\alpha = 25$ deg, the inboard shift of the WLVs, CLVs, and CTVs, both strongly connected by their shear layers, accounts for the two regions of maximum rms values (Fig. 8b). The pattern of $\Delta c_{p_{\mathrm{rms}}}$ is significantly changed at $\alpha = 30$ deg (Fig. 9c). The fin encounters high-pressure fluctuations increasing from the root to the tip, where a maximum exists close to the trailing edge. The source of this maximum is the unsteadiness produced by the inboard part of the WLV sheet touching the midsection.

At $\beta = 5$ and $\alpha = 20$ deg, the behavior in $\Delta c_{p_{\mathrm{rms}}}$ is such that two regions of increased pressure fluctuations are present (Fig. 9a). They are evoked by vortices emanating from the canopy and canard. The pattern of $\Delta c_{p_{\mathrm{rms}}}$ is completely different at $\alpha = 25$ deg (Fig. 9b). There, the largest rms values are in a midspan region that covers the whole local chord. With increasing α, this region is shifted upward, being extended at the same time. At $\alpha = 30$ deg, the peak values reach levels up to 32% (Fig. 9c).

To verify the results of the lifting surface method, $c_{p_{\mathrm{rms}}}$ is compared with that of unsteady pressure measurements.[29] The standard fin was replaced by an extensively instrumented fin,

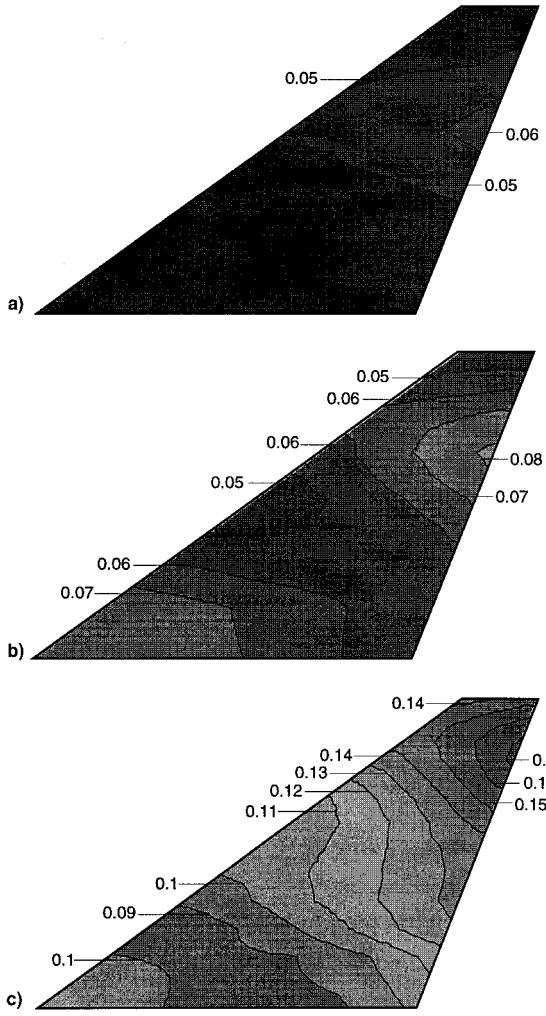

Fig. 8 Contours of $\Delta c_{p_{rms}}$ at α = a) 20, b) 25, and c) 30 deg and β = 0 deg. 6 × 15 collocation points.

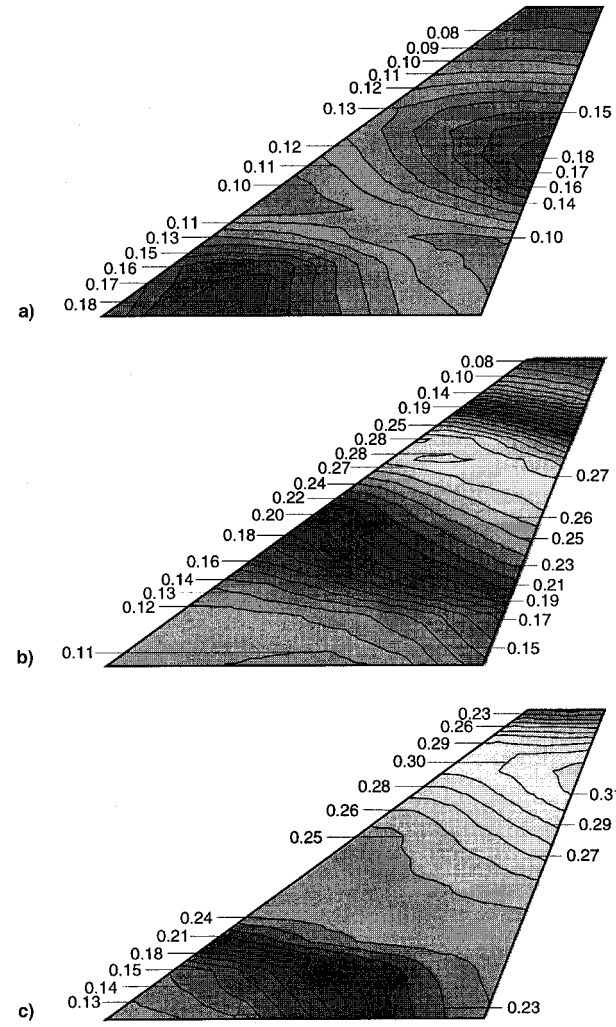

Fig. 9 Contours of $\Delta c_{p_{rms}}$ at α = a) 20, b) 25, and c) 30 deg and β = 5 deg. 6 × 15 collocation points.

equipped with 24 Kulite XCQ-062-1.7 bar A pressure transducers. The pressure signals were sampled at 12 positions directly opposite each other on each surface (Fig. 10). Test conditions refer to $Ma = 0.5$, $q_\infty = 14.9$ kPa, and $Re = 3.0 \times 10^6$. The pressure signals were amplified, bandpass filtered with a low cutoff frequency of 5 Hz, a high cutoff frequency of 1000 Hz, and digitized with 12-bit precision. The sampling rate for each channel was 6250 Hz, providing 8000 samples within 1.28 s. The comparison between pressure and flowfield measurements is limited by the fact that test configurations of the model slightly differ. At pressure measurements wing leading- and trailing-edge flap deflections were set to −20, and 20 deg, respectively, and the canard setting angle was set to −10 deg. At flowfield measurements all settings were 0 deg.

For the lifting surface method, values of $c_{p_{rms}}$ related to one side of the fin are obtained by $c_{p_{rms}} = \frac{1}{2}\Delta c_{p_{rms}}$. This is based on the conservative assumption that the amplitude functions of fluctuating pressure at stations opposite each other act with the same mode. Both measured and calculated $c_{p_{rms}}$ are averaged for one side and plotted together as a function of angle of attack (Fig. 10). For averaging $c_{p_{rms}}$ panels are used (Figs. 2 and 10), assuming that rms pressures are constant throughout the panels

$$c_{p_{rms}} = \sum_{i=1}^{N_p} c_{p_{rms},i} \frac{A_{P_i}}{A_F} \tag{12}$$

For the calculated $c_{p_{rms}}$, a vertical bar represents the scope of the respective minimum and maximum, whereas the gray-colored area reflects the range of minimum and maximum measured values. At symmetric freestream there is an excellent agreement between measured and calculated values of $c_{p_{rms}}$. As concluded from the contour plots the magnitude of pressure fluctuations increases significantly above α = 25 deg.

At β = 5 deg, the values of $c_{p_{rms}}$ obtained with the lifting surface code corresponds to the measured values of the port (leeward) side (Fig. 11). The calculations are based on flowfield measurements performed with the fin section removed, where the starboard vortex systems mainly dominate the fin flow without any surface interference. For the fin-on case it seems that interference effects result in increased pressure fluctuations on the port (suction) side. However, the amplitudes of fluctuating fin local incidence found for the fin region at fin-off and fin-on do not show significant differences.[31] Consequently, the calculated values of $c_{p_{rms}}$ match at moderate α with the measured ones of the port side. At high α, the averaged values of calculated $c_{p_{rms}}$ show higher levels than those gained from the measurements, but they are below the maximum measured values.

Spectral Content of Calculated Buffet Loads

Figure 12 depicts power spectral densities of fluctuating differential pressure at station A 17 for all angles of attack investigated and β = 0 deg. A plot of spanwise spectra at X = 0.44 is shown for α = 28 and β = 0 deg (Fig. 13). In all cases the frequency resolution is 1.95 Hz. At $\alpha \geq 25$ deg, the spectra exhibit dominant frequencies varying with angle of attack. Because of the linear relationship between the oscillations of local

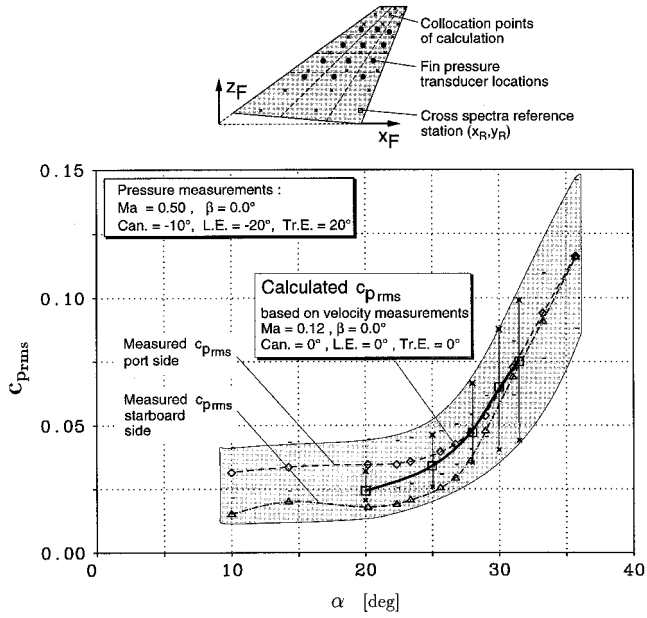

Fig. 10 Calculated compared with direct measured rms fin surface pressure as a function of angle of attack at β = 0 deg. 3 × 8 collocation points.

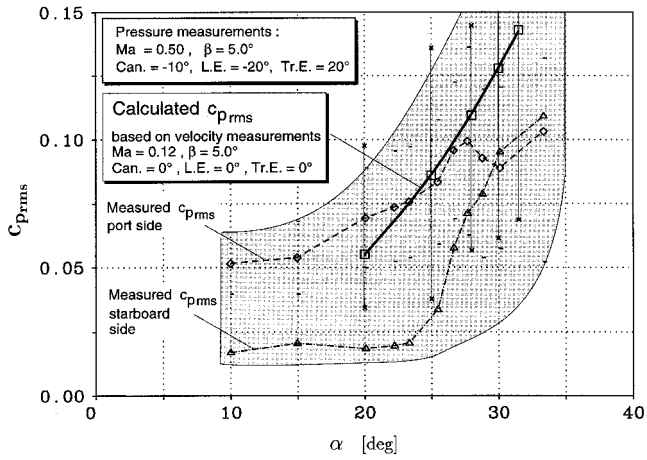

Fig. 11 Calculated compared with direct measured rms fin surface pressure as a function of angle of attack at β = 5 deg. 3 × 8 collocation points.

incidence and pressure, the peaks in pressure spectral densities coincide with the frequency peaks detected in the velocity spectra. At a fixed angle of attack the center frequency of the peaks changes slightly with the different stations, whereas the content of turbulent kinetic energy differs significantly (Fig. 13).

From the discussion of the pressure field and the related spectra it is seen that for a detailed description of the buffet loads a large number of surface positions must be summed. The lifting surface method provides total buffet loads from pressure integration. For various α and β = 0 deg, the normal-force coefficient spectra show that the pressure field contains energy over a moderately wide frequency range (Fig. 14). A peak can be detected at the same value of reduced frequency as in the pressure spectra.

Dominant Frequency

The variation of the buffet load dominant frequency with angle of attack is summarized in Fig. 15. The dominant frequency decreases with α from $k = 0.8$ at α = 25 deg to $k = 0.61$ at α = 31.5 deg. To scale for angle of attack a reduced frequency k' is used, based on the wing root chord and the

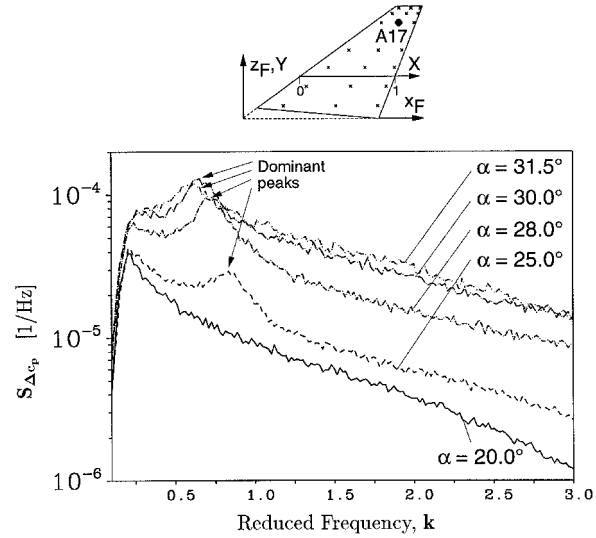

Fig. 12 Spectra of $S_{\Delta c_p}$ at collocation point A 17 ($X = 0.611$, $Y = 0.831$) for various angles of attack at β = 0 deg.

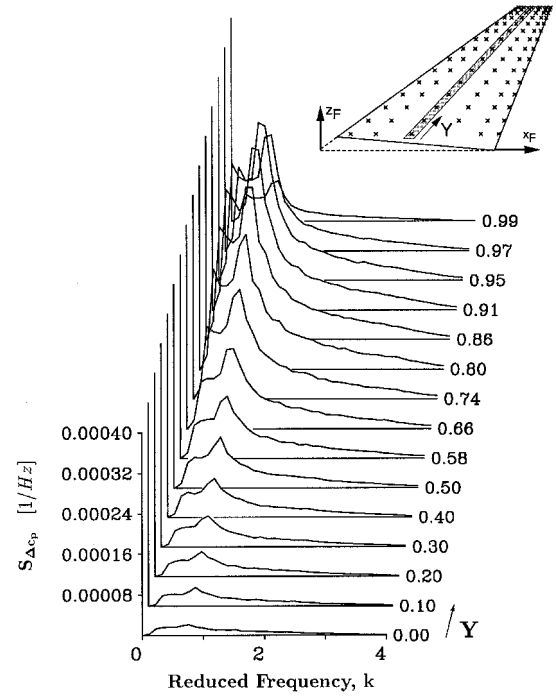

Fig. 13 Spectra of $S_{\Delta c_p}$ for various spanwise stations at $X = 0.44$, and α = 28 and β = 0 deg.

sinus of α. For different α, the values of k match at $k' = 0.48$. Regarding a survey normal to freestream[4,5] the volume of the burst leading-edge vortex increases with angle of attack, and so the frequency of the related quasiperiodic fluctuations decrease.

An excellent agreement can be shown again when comparing the values of k' based on the calculation with those obtained from the pressure measurements[29] (Fig. 16). For a flexible aircraft, a large structural response could result from the peak in the buffet load spectra, which varies with frequency, dynamic pressure, and angle of attack. This occurs when the pronounced frequency of the buffet loads coincides approximately with one of the fin natural frequencies. If the buffet load dominant frequencies are well known at an early design stage, the structural properties can be chosen in a way that tuning of the peak in the buffet load spectra with any of the natural frequencies of the fin is avoided.

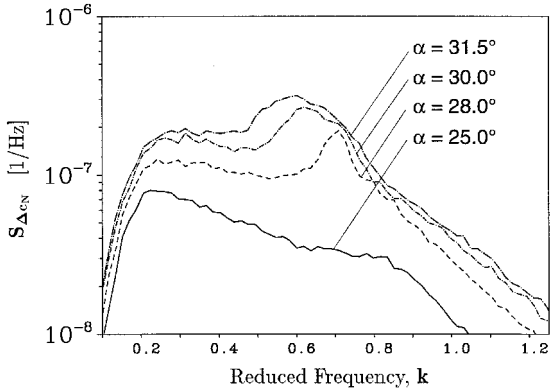

Fig. 14 Spectra of $S_{\Delta c_N}$ for various angles of attack at β = 0 deg.

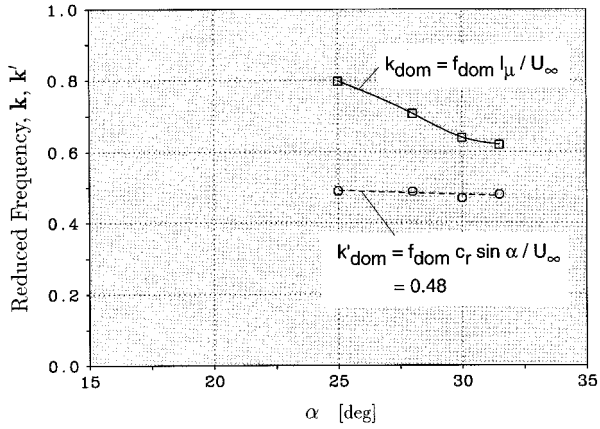

Fig. 15 Dominant reduced frequency of fin buffet load as function of angle of attack at β = 0 deg.

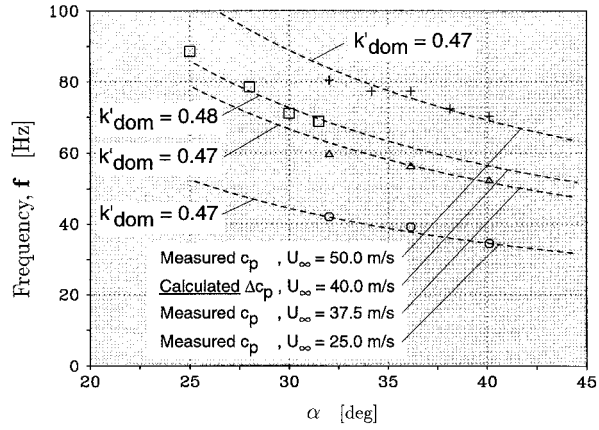

Fig. 16 Dominant reduced frequency of fin buffet load obtained from calculation and pressure measurements as function of angle of attack and freestream velocity at β = 0 deg.

Conclusions

A prediction method for fin buffet aerodynamic loads was presented to evaluate unsteady fin surface pressure on a single-finned, delta-canard configuration in the range of α = 20 to 31.5 deg and at β = 0 and 5 deg. The method is based on fluctuating flowfield velocity using a modified lifting surface code. The buffet excitation input was shown to be characterized by increased turbulence intensity with peaked velocity spectra. From the lifting surface method, rms values and spectra of fluctuating pressure and normal force were obtained. It was clearly shown that with increasing incidence there is an evident increase in unsteady pressure. The pattern of intensity of the pressure fluctuations changes strongly with α, depending mainly on the development and interaction of the wing and CLV systems. Normal force spectra exhibit a distinct narrowband peak that varies with the angle of attack corresponding to that of the velocity spectra. A correlation of the peak reduced frequency with the sinus of α gives a value of 0.48. The calculated rms pressures were compared with those of pressure measurements. At symmetric freestream an excellent agreement was shown for all α investigated. At sideslip and moderate angle of attack, the calculated fin buffet loads matches with those measured on the leeward side. At high α, averaged fin buffet loads would be overestimated but are below the level of maximum measured values. It is thought that the method presented will be able to predict buffet load characteristics already at an early design stage.

Acknowledgments

This work was supported in part by the Daimler–Benz Aerospace AG (DASA) under the directorat of W. Kuny. The authors express their appreciation to J. Becker (DASA) for his kind assistance in the research project.

References

[1]Mabey, D. G., and Pyne C. R., "Fin Buffeting at High Angles of Incidence on a Model of Slender Wing Aircraft," *Proceedings of the International Forum on Aeroelasticity and Structural Dynamics* (Aachen, Germany), 1991, pp. 552–561 (Paper 91-129).

[2]Lee, B. H. K., Brown, D., Tang, F. C., and Plosenski, M., "Flowfield in the Vicinity of an F/A-18 Vertical Fin at High Angles of Attack," *Journal of Aircraft*, Vol. 30, No. 1, 1993, pp. 69–74.

[3]Del Frate, J. H., and Zuniga, F. A., "In-Flight Flow Field Analysis on the NASA F-18 High Alpha Research Vehicle with Comparisons to Ground Facility Data," AIAA Paper 90-0231, Jan. 1990.

[4]Breitsamter, C., and Laschka, B., "Turbulent Flow Structure Associated with Vortex-Induced Fin Buffeting," *Journal of Aircraft*, Vol. 31, No. 4, 1994, pp. 773–781.

[5]Breitsamter, C., and Laschka, B., "Turbulent Flowfield Structure Associated with Fin Buffeting Around a Vortex-Dominated Aircraft Configuration at Sideslip," *Proceedings of the 19th Congress of the International Council of the Aeronautical Sciences* (Anaheim, CA), Vol. 1, 1994, pp. 768–784 (ICAS Paper 94-4.3.2).

[6]Ferman, M. A., Patel, S. R., Zimmermann, N. H., and Gerstenkorn, G., "A Unified Approach to Buffet Response of Fighter Aircraft Empennage," *Aircraft Dynamic Loads Due to Flow Separation* (Sorrento, Italy), 1990, pp. 2-1–2-18 (AGARD-CP-483).

[7]Zimmermann, N. H., Ferman, M. A., Yurkovich, R. N., and Gerstenkorn, G., "Prediction of Tail Buffet Loads for Design Applications," Rept. NADC-880434-60, July 1987.

[8]Zimmermann, N. H., Ferman, M. A., Yurkovich, R. N., and Gerstenkorn, G., "Prediction of Tail Buffet Loads for Design Applications," AIAA Paper 89-1378, April 1989.

[9]Ashley, H., Rock, S. M., Digumarthi, R. V., Chaney, K., and Eggers, A. J., Jr., "Active Control for Fin Buffet Allevation," U.S. Air Force Wright Lab., WL-TR-93-3099, Wright–Patterson AFB, OH, Jan. 1994.

[10]Mayori, A., and Rockwell, D., "Interaction of a Streamwise Vortex with a Thin Plate: A Source of Turbulent Buffeting," *AIAA Journal*, Vol. 32, No. 10, 1994, pp. 2022–2029.

[11]Canbazoglu, S., Lin, J.-C., Wolfe, S., and Rockwell, D., "Buffeting of a Fin: Streamwise Evolution of Flow Structure," *Journal of Aircraft*, Vol. 33, No. 1, 1995, pp. 185–190.

[12]Canbazoglu, S., Lin, J.-C., Wolfe, S., and Rockwell, D., "Buffeting of a Fin: Distortion of Incident Vortex," *AIAA Journal*, Vol. 33, No. 11, 1995, pp. 2144–2150.

[13]Wolfe, S., Canbazoglu, S., Lin, J.-C., and Rockwell, D., "Buffeting of Fins: An Assessment of Surface Pressure Loading," *AIAA Journal*, Vol. 33, No. 11, 1995, pp. 2232–2235.

[14]Triplett, W. E., "Pressure Measurements on Twin Vertical Tails in Buffeting Flow," *Journal of Aircraft*, Vol. 20, No. 11, 1983, pp. 920–925.

[15]Lee, B. H. K., and Brown, D., "Wind-Tunnel Studies of F/A-18 Tail Buffet," *Journal of Aircraft*, Vol. 29, No. 1, 1992, pp. 146–152.

[16]Hebbar, S. K., Platzer, M. F., and Liu, D.-M., "Effect of Canard Oscillations on the Vortical Flowfield of a X-31A-Like Fighter Model in Dynamic Motion," AIAA Paper 93-3427, Jan. 1993.

[17]Colvin, B. J., Mullans, R. E., Paul, R. J., and Ross, H. N., "F-15

Vertical Tail Vibration Investigations," McDonnell Douglas Corp., Rept. A6114, McDonnell Aircraft Co., St. Louis, MO, Sept. 1979.

[18]Lee, B. H. K., and Tang, F. C., "Unsteady Pressure and Load Measurements on a F/A-18 Vertical Fin," *Journal of Aircraft*, Vol. 30, No. 5, 1993, pp. 228–234.

[19]Martin, C. A., Glaister, M. K., MacLaren, L. D., Meyn, L. A., and Ross, S., "F/A-18 1/9th Scale Model Tail Buffet Measurements," Dept. of Defence, Aeronautical Research Lab., Flight Mechanics, Rept. 188, Melbourne, Victoria, Australia, June 1991.

[20]Shah, G. H., "Wind Tunnel Investigation of Aerodynamic and Tail Buffet Characteristics of Leading-Edge Extension Modifications to the F/A-18," *Proceedings of the AIAA Atmospheric Flight Mechanics Conference*, AIAA, Washington, DC, 1991, pp. 395–412.

[21]Meyn, L. A., Lanser, W. R., and James, K. D., "Full-Scale High Angle-of-Attack Tests of an F/A-18," AIAA Paper 92-2676, June 1992.

[22]Lee, B. H. K., Brown, D., Zgela, M., and Poirel, D., "Wind Tunnel Investigations and Flight Tests of Tail Buffet on the CF-18 Aircraft," *Aircraft Dynamic Loads Due to Flow Separation* (Sorrento, Italy), 1990, pp. 1-1–1-26 (AGARD-CP-483).

[23]Breitsamter, C., "Experimentelle Untersuchung der instationären Feldgrößen und Oberflächendrücke bei wirbeldominierter abgelöster Strömung," *Deutscher Luft- und Raumfahrtkongreß*, Vol. I, DGLR-Jahrestagung, DGLR-JT95-062, Bonn-Bad Godesberg, 1995, pp. 163–175.

[24]Rizk, Y. M., and Gee, K., "Unsteady Simulation of Viscous Flow Field Around F-18 Aircraft at Large Incidence," *Journal of Aircraft*, Vol. 29, No. 6, 1992, pp. 986–992.

[25]Kandil, O. A., Sheta, E. F., and Liu, C. H., "Computation and Validation of Fluid/Structure Twin Tail Buffet Response," *Euromech-Colloquium 349, Simulation of Structure Fluid Interaction in Aeronautics* (Göttingen, Germany), 1996, pp. 15-1–15-10.

[26]Lee, B. H. K., "A Method for Predicting Wing Response to Buffet Loads," *Journal of Aircraft*, Vol. 21, No. 1, 1984, pp. 85–87.

[27]Laschka, B., "Zur Theorie der harmonisch schwingenden tragenden Fläche bei Unterschallanströmung," *Zeitschrift für Flugwissenschaften*, 11. Jahrgang, Heft 7, Juli 1963, pp. 261–292.

[28]Breitsamter, C., and Laschka B., "Velocity Measurements with Hot-Wires in a Vortex-Dominated Flowfield," *Wall Interference, Support Interference and Flow Field Measurements* (Brussels, Belgium), 1993, pp. 11-1–11-13 (AGARD-CP-535).

[29]Breitsamter, C., "Turbulente Strömungsstrukturen an Flugzeugkonfigurationen mit Vorderkantenwirbeln," Ph.D. Dissertation, Technische Universität München, Germany, 1997.

[30]Breitsamter, C., "Messungen und Analyse der zeitabhängigen Geschwindigkeiten im wirbeldominierten Strömungsfeld eines Hochleistungsflugzeugs, Teil 2," FLM-91/54, Lehrstuhl für Fluidmechanik, Technische Universität München, Germany, 1991.

[31]Wittmann, A., and Breitsamter, C., "Experimentelle Untersuchung des Strömungsfeldes im Bereich des Seitenleitwerks einer Delta-Canard-Konfiguration," FLM-93/25, Lehrstuhl für Fluidmechanik, Technische Universität München, Germany, 1993.

[32]Watkins, C. E., Runyan, H. L., and Woolston, D. S., "On the Kernel Function of the Integral Equation Relating the Lift and Downwash Distributions of Oscillating Finite Wings in Subsonic Flow," NACA TR 1234, 1955.

[33]Lee, B. H. K., and Tang, F. C., "Characteristics of the Surface Pressures on a F/A-18 Vertical Fin Due to Buffet," *Journal of Aircraft*, Vol. 31, No. 1, 1994, pp. 228–234.

[34]Bendat, J. S., and Piersol, A. G., *Random Data: Analysis and Measurement Procedures*, Wiley, New York, 1971.